

Gate-tunable carbon nanotube–MoS₂ heterojunction p-n diode

Deep Jariwala^a, Vinod K. Sangwan^a, Chung-Chiang Wu^a, Pradyumna L. Prabhurashi^a, Michael L. Geier^a, Tobin J. Marks^{a,b,1}, Lincoln J. Lauhon^a, and Mark C. Hersam^{a,b,c,1}

Departments of ^aMaterials Science and Engineering, ^bChemistry, and ^cMedicine, Northwestern University, Evanston, IL 60208

Contributed by Tobin J. Marks, September 12, 2013 (sent for review August 13, 2013)

The p-n junction diode and field-effect transistor are the two most ubiquitous building blocks of modern electronics and optoelectronics. In recent years, the emergence of reduced dimensionality materials has suggested that these components can be scaled down to atomic thicknesses. Although high-performance field-effect devices have been achieved from monolayered materials and their heterostructures, a p-n heterojunction diode derived from ultrathin materials is notably absent and constrains the fabrication of complex electronic and optoelectronic circuits. Here we demonstrate a gate-tunable p-n heterojunction diode using semiconducting single-walled carbon nanotubes (SWCNTs) and single-layer molybdenum disulfide as p-type and n-type semiconductors, respectively. The vertical stacking of these two direct band gap semiconductors forms a heterojunction with electrical characteristics that can be tuned with an applied gate bias to achieve a wide range of charge transport behavior ranging from insulating to rectifying with forward-to-reverse bias current ratios exceeding 10⁴. This heterojunction diode also responds strongly to optical irradiation with an external quantum efficiency of 25% and fast photoresponse <15 μs. Because SWCNTs have a diverse range of electrical properties as a function of chirality and an increasing number of atomically thin 2D nanomaterials are being isolated, the gate-tunable p-n heterojunction concept presented here should be widely generalizable to realize diverse ultrathin, high-performance electronics and optoelectronics.

2D transition metal dichalcogenide | single layer MoS₂ | van der Waals heterostructure | rectifier | photodetector

When two semiconductors with an opposite carrier type contact one another, charge transfer occurs across their interface and creates a potential difference determined by the doping profile. In bulk semiconductor p-n junctions, the doping level is primarily controlled via diffusion or implantation of substitutional impurities, which implies minimal control over the doping profile following device fabrication. In contrast, atomically thin semiconductors can be electrostatically doped by applying a bias to a capacitively coupled gate electrode (1–3). The atomically thin structure of these materials also enables doping modulation of the overlying layers in a vertically stacked heterostructure (4). For example, this strategy allows gapless graphene to be used in field-effect tunneling devices in combination with other layered materials (4, 5). Vertical 2D heterostructures have also been used to create high-performance Metal Oxide Semiconductor Field Effect Transistors (MOSFETs) (6), tunneling field-effect transistors (FETs) (4), barristors (7), inverters (8), and memory devices (9, 10), in addition to facilitating the study of novel physical phenomena in layered materials (11–14). Similarly, in-plane graphene heterostructures and controlled doping have served as the basis for unique 2D devices (15–18). Although the nearly perfect 2D structure and low density of states in graphene provide advantages in some heterostructure devices, its gapless nature prevents the formation of a large potential barrier for charge separation and current rectification despite efforts to create in-plane p-n homojunctions by split gating (19). In particular, the lack of distinct monolayer

semiconductors with complementary (p and n) polarities has precluded the realization of a gate-tunable heterojunction p-n diode.

In this report, we demonstrate the fabrication and operation of a gate-tunable p-n heterojunction diode using semiconducting single-walled carbon nanotubes (s-SWCNTs) (p-type) (20) and single layer (SL)-MoS₂ (n-type) (21, 22). Fig. 1A shows a false-colored SEM of a representative device. A lower-magnification optical micrograph of the same device in Fig. 1B shows the n-type (SL-MoS₂) FET, p-n s-SWCNT/SL-MoS₂ heterojunction, and p-type (s-SWCNT) FET from top to bottom. The device fabrication begins by depositing e-beam lithographically defined gold electrodes on SL-MoS₂ flakes that are exfoliated on 300-nm SiO₂/Si wafers (Fig. 1C, I). The SL-MoS₂ FET is electrically isolated by patterning 30-nm alumina via atomic layer deposition (ALD) followed by transfer and patterning of a sorted s-SWCNT thin film (23, 24) (Fig. 1C, II) to yield the final device (Fig. 1C, III). *SI Text* provides further details on the device fabrication.

The ultrathin nature of the heterojunction allows gate tunability of the diode electrical characteristics. Fig. 2A shows the output plots of a representative device under different gate biases. The device transitions from a nearly insulating behavior at $V_G = 70$ V to a poorly rectifying state ($r^2 < 60\%$ for fits to the Shockley diode equation) at $V_G = 40$ V to a highly rectifying diode for $V_G \leq 0$ V ($r^2 > 99\%$). For the heterojunction diodes, V_D refers to the bias on the s-SWCNT electrode such that $V_D > 0$ corresponds to forward bias while the electrode in contact with SL-MoS₂ is grounded. The transfer plot further demonstrates the gate tunability of the current through the p-n heterojunction (Fig. 2B). The transfer characteristics of the junction (green)

Significance

The p-n junction diode is the most ubiquitous and fundamental building block of modern electronics, with far-reaching applications including integrated circuits, detectors, photovoltaics, and lasers. With the recent discovery and study of atomically thin materials, opportunities exist for adding new functionality to the p-n junction diode. Here we demonstrate that a p-n heterojunction diode based on atomically thin MoS₂ and sorted semiconducting carbon nanotubes yields unprecedented gate tunability in both its electrical and optical properties, which is not observed in the case of bulk semiconductor devices. In addition to enabling advanced electronic and optoelectronic technologies, this p-n heterojunction diode provides new insight into charge transport and separation at atomically thin heterointerfaces.

Author contributions: D.J., V.K.S., T.J.M., L.J.L., and M.C.H. designed research; D.J., V.K.S., C.-C.W., P.L.P., and M.L.G. performed research; D.J., V.K.S., C.-C.W., L.J.L., and M.C.H. analyzed data; and D.J., V.K.S., C.-C.W., P.L.P., M.L.G., T.J.M., L.J.L., and M.C.H. wrote the paper.

The authors declare no conflict of interest.

¹To whom correspondence may be addressed. E-mail: t-marks@northwestern.edu or m-hersam@northwestern.edu.

This article contains supporting information online at www.pnas.org/lookup/suppl/doi:10.1073/pnas.1317226110/-DCSupplemental.

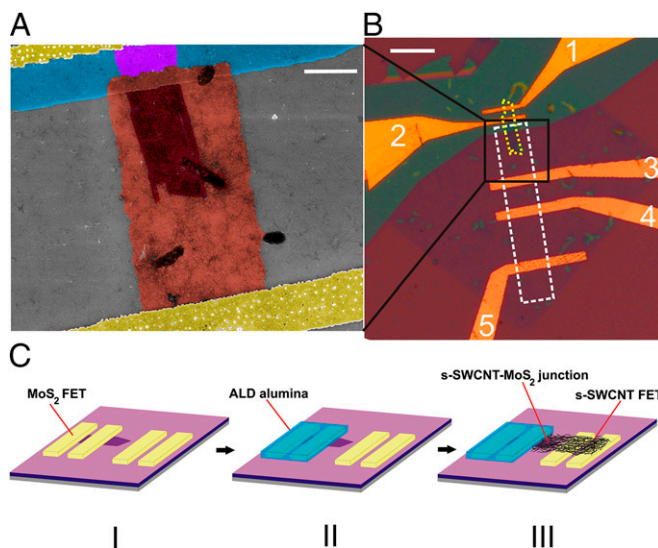


Fig. 1. Microscopy and fabrication of the s-SWCNTs/SL-MoS₂ p-n heterojunction diode. (A) False-colored SEM image of the heterojunction diode. (Scale bar, 2.5 μm .) The yellow regions at the top and bottom are the gold electrodes. The patterned alumina (blue region) serves as a mask for insulating a portion of the SL-MoS₂ flake (violet region). The pink region is the patterned random network of s-SWCNTs (p-type) in direct contact with the exposed part of the SL-MoS₂ flake (n-type) to form the p-n heterojunction diode (dark red). (B) Optical micrograph showing the device layout at a lower magnification. The dashed yellow boundary indicates the SL-MoS₂ flake, whereas the dashed white rectangle denotes the patterned s-SWCNT film. Electrodes 1 and 2 form the n-type (SL-MoS₂) FET, which is insulated by the patterned alumina film (cyan). Electrodes 2–3 form the p-n heterojunction, whereas 3–4 and 4–5 form p-type s-SWCNT FETs. (Scale bar, 10 μm .) (C) Schematic of the fabrication process: (I) SL-MoS₂ FET and an extra pair of electrodes are fabricated via e-beam lithography on 300 nm SiO₂/Si. The Si substrate acts as the global back gate. (II) The MoS₂ FET is insulated by patterning an alumina film in a liftoff process, followed by (III) transfer and patterning of the s-SWCNT network to yield the final device configuration consisting of a top contact SL-MoS₂ FET, bottom contact s-SWCNT FET, and p-n heterojunction.

show an unusual gate voltage dependence, which we refer to as “antiambipolar” behavior. In particular, the maximum conductance occurs near $V_G = 0$, which is the opposite of conventional ambipolar behavior that shows a minimum conductance near $V_G = 0$. The current on/off ratio exceeds 10^4 in the transfer plots, which is suitable for advanced logic applications (SI Text). The transfer characteristics of the heterojunction can be qualitatively viewed as a superposition of the p-type s-SWCNT (red) and n-type SL-MoS₂ (blue) FET transfer plots. However, the net current through the heterojunction is smaller than the SL-MoS₂ and s-SWCNT FET transfer characteristics due to the additional resistance at the junction.

This unique transfer characteristic can be viewed as originating from an FET channel consisting of two p and n semiconductors in series. The change in the resistance of each component with gate bias affects the net series resistance leading to the resulting antiambipolar transfer characteristic of the junction. Thus, the junction transfer curve has two off states, representing the depleted state of SL-MoS₂ and s-SWCNTs. Furthermore, the contact resistances of the s-SWCNT film and SL-MoS₂ with Au are relatively small compared with the sheet/channel resistances (25, 26) and thus have negligible effect on the junction characteristics (see SI Text for output plots of s-SWCNT and SL-MoS₂ FETs). It is worth noting that the maximum of the junction transfer curve does not exactly coincide with the intersection of the SL-MoS₂ and s-SWCNT transfer curves. This offset can be attributed to hysteresis in the transfer

plots and the fact that the SL-MoS₂ FET is encapsulated in alumina, which is known to shift threshold voltage in SL-MoS₂ FETs (21).

An important parameter in characterizing diode characteristics is the ratio of the forward current, I_f/I_r , to the reverse current, I_r/I_f , at the same bias magnitude. Fig. 2C shows that I_f/I_r varies by over five orders of magnitude as a function of gate voltage. Between the two gate bias extremes, the s-SWCNT/SL-MoS₂ heterojunction transitions from an n-n⁺ junction at $V_G = 80$ V to a p-n junction at $V_G = -80$ V. The large band gap of SL-MoS₂ (>1.8 eV) (27) compared with that of the s-SWCNTs (~0.7 eV) allows electrostatic depletion of SL-MoS₂ to a lightly n-doped (n⁻) or nearly intrinsic insulating state, thereby leading to I_f/I_r values exceeding 10^4 at $V_G = -80$ V. On the other hand, the small band gap of the s-SWCNTs allows electrostatic inversion from p-doping to n-doping at large positive V_G , resulting in poor I_f/I_r values for $V_G > 60$ V. Gate tunable p-n homojunction diodes have been previously fabricated by split gating of individual SWCNTs. However, such homojunctions only allow control over the built-in voltage via differential biases in split gates (28, 29). The present gate tunable p-n heterojunction, on the other hand, is fundamentally different as it has a built-in potential at zero gate bias as evident from the rectifying current (I -voltage (V)) (I - V) characteristics (Fig. 24). Furthermore, in this heterojunction, the gate is used to simultaneously tune the doping concentrations of both semiconductors, thereby allowing tunability in the built-in voltage and rectification ratios.

To further understand the gate-dependent modulation of the heterojunction I - V curves, we fit them to the Shockley diode equation. The best fit to the Shockley diode equation is observed for $V_G = -40$ V. For other V_G values, either the diode ideality factor (n) is >2 or the fits are poor ($r^2 < 60\%$) (SI Text). The disorder at the interface of random network SWCNT films [see atomic force microscopy (AFM) images in SI Text] and SL-MoS₂ possibly leads to more recombination, resulting in larger ideality factors compared with the nearly ideal diode behavior in WSe₂/InAs heterojunctions that have a uniform 2D interface (30). The gate dependence of the present diode behavior enables gate-tunable rectifier circuits (Fig. 2D), which is a unique feature of the s-SWCNT/SL-MoS₂ heterojunction device that has not been observed in conventional bulk semiconductor diodes (see SI Text for further details on measurement techniques).

Both SL-MoS₂ and s-SWCNTs have direct band gaps (31, 32) and exhibit signatures of bound excitonic states in their absorption spectra (2, 31). Therefore, photocurrent generation is expected on optical irradiation of p-n heterojunctions based on these materials. To that end, scanning photocurrent microscopy was used to spatially map the local photoresponse of the s-SWCNT/SL-MoS₂ heterojunction device (Fig. 3A). The regions of large negative photocurrent lie in the heterojunction area outlined by the SL-MoS₂ flake (purple) overlapping with the patterned s-SWCNT film (red). No measurable photocurrent is observed from the nonoverlapping regions of either the s-SWCNT film, SL-MoS₂, or the electrical contacts (see SI Text for additional details), indicating that the photocurrent measured under uniform illumination is generated by the vertical heterojunction. Photocurrent from Au contacts to s-SWCNT films was not observed in our recent study (33). For the case of two-terminal SL-MoS₂ devices, photocurrent has been observed at the contacts due to band bending (34). However, the band bending at the contacts is opposite to that of the junction, which suppresses the local near-contact photocurrent because charge neutrality cannot be maintained at the injection level used. The spectral dependence of the photocurrent (Fig. 3B) corresponds to the absorption peaks of SL-MoS₂ (27) and S₂₂ (24) peaks of s-SWCNTs, which demonstrates that this unique heterointerface can induce carrier separation following exciton and/or free carrier generation in either material. The photocurrent generated in the visible portion of the

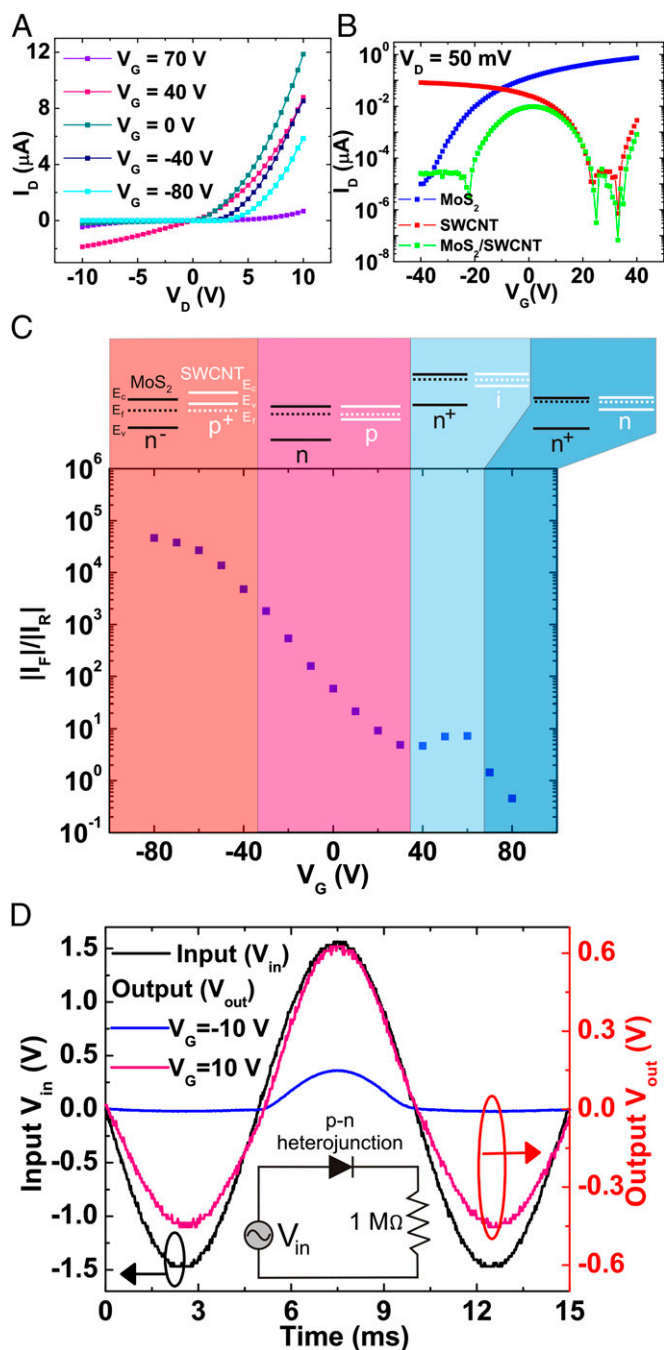


Fig. 2. Electrical properties of the s-SWCNT/SL-MoS₂ p-n heterojunction diode. (A) Gate-tunable output characteristics showing the transition from a nearly insulating state at $V_G = 70$ V to a conductive state with relatively poor rectification at $V_G = 40$ V to a highly rectifying diode behavior at negative gate voltages. (B) Transfer characteristics of the p-n junction (green), showing an antiambipolar characteristic, which is qualitatively a superposition of the transfer characteristics of the p-type s-SWCNT FET and n-type SL-MoS₂ FET. (C) Forward-to-reverse current ratio (at a heterojunction bias magnitude of 10 V) as a function of gate bias. The labels at the top show the corresponding band diagrams for the s-SWCNT/SL-MoS₂ p-n heterojunction. At a high positive gate bias, the formation of an n⁺-i junction implies a low rectification ratio that transitions into an n⁺-i junction (plateau region in the plot) with reducing V_G . The rectification ratio then rises with decreasing gate bias due to the formation of a p-n junction. (D) Demonstration of gate-tunable rectification using the p-n heterojunction diode. The y axis on the left shows the input voltage, whereas the y axis on the right shows the output voltage across the series resistor (1 M Ω). As a function of the gate bias, the device evolves from a nonrectifying resistor-like state at $V_G = 10$ V (magenta) to a diode-like rectifying state at $V_G = -10$ V (blue).

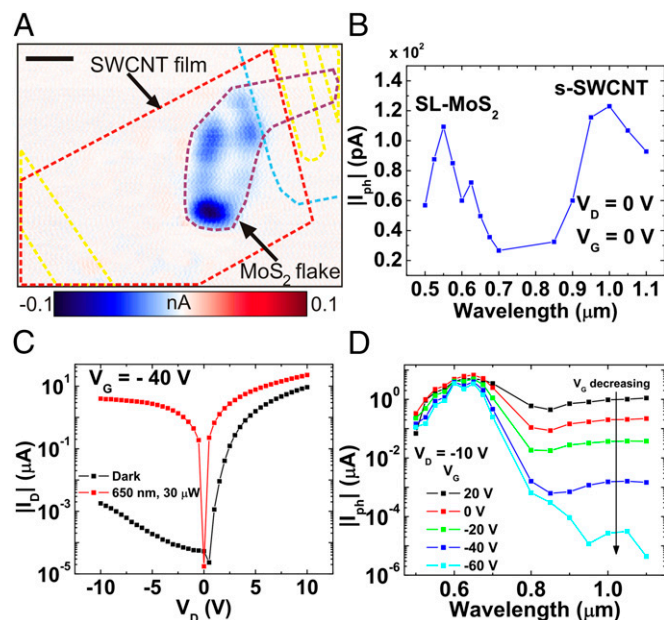


Fig. 3. Photoresponse of the p-n heterojunction. (A) Scanning photocurrent micrograph of a representative heterojunction device acquired at V_D (s-SWCNT electrode), $V_G = 0$ V showing the outlines of the SL-MoS₂ flake (purple dashed line) and the patterned s-SWCNT film (red dashed line) acquired at 700 nm with 20- μ W power. Regions of large negative photocurrent (blue) are observed in the overlapping junction region. The patterned alumina and electrodes are indicated by cyan and yellow dashed lines, respectively. (B) Photocurrent spectrum of the junction under global illumination and zero bias conditions. The photocurrent magnitude is highest at the characteristic absorption energies of both SL-MoS₂ and s-SWCNTs. The photocurrent spectrum is acquired at the same incident power (30 μ W). (C) Output curve of the same device in the dark and under global illumination at 650 nm. (D) Photocurrent spectral response can be tuned with the gate voltage. With decreasing gate voltage, the increased p-doping of the nanotubes and concomitant decreased n-doping of MoS₂ leads to a lower photocurrent in the near-infrared region.

spectrum also likely has contributions from both SL-MoS₂ and the S₃₃ transitions of s-SWCNTs because both absorb in that range of wavelengths (see *SI Text* for absorbance spectrum of SWCNTs).

To further illustrate the photoresponse of the s-SWCNT/SL-MoS₂ heterojunction, both output (I - V) and transfer curves (I - V_G) were acquired under global illumination at a series of wavelengths. A representative comparison of the dark and illuminated I - V curves at $V_G = -40$ V reveals that the photocurrent increases by four orders of magnitude at a heterojunction reverse bias of -5 V (Fig. 3C). Fig. 3D also shows the gate voltage-dependent photocurrent values at a heterojunction reverse bias of -10 V (Fig. 3D). As the gate voltage becomes more negative, the relative contribution from the s-SWCNT portion of the spectrum decreases, which is consistent with the s-SWCNT/SL-MoS₂ heterojunction becoming a p⁺-n⁻ junction. Because the depletion region in a p-n junction extends farther into the side with lower doping/majority carrier concentration, the junction almost entirely lies in the SL-MoS₂ as it is depleted at negative V_G , leading to a reduced photocurrent contribution from the s-SWCNTs as observed in Fig. 3D. If we consider the junction from a molecular perspective used to describe organic semiconductor heterojunctions, one might also expect a change in the rate of charge transfer due to changes in band offsets [or Highest Occupied Molecular Orbitals (HOMO) and Lowest Unoccupied Molecular Orbitals (LUMO) levels] across the heterojunction.

With a strong photoresponse, the s-SWCNT/SL-MoS₂ heterojunction can be exploited as a photodetector. Diode-based

22. Jariwala D, et al. (2013) Band-like transport in high mobility unencapsulated single-layer MoS₂ transistors. *Appl Phys Lett* 102(17):173107.
23. Sangwan VK, et al. (2012) Fundamental performance limits of carbon nanotube thin-film transistors achieved using hybrid molecular dielectrics. *ACS Nano* 6(8):7480–7488.
24. Arnold MS, Green AA, Hulvat JF, Stupp SI, Hersam MC (2006) Sorting carbon nanotubes by electronic structure using density differentiation. *Nat Nanotechnol* 1(1):60–65.
25. Behnam A, et al. (2013) High-field transport and thermal reliability of sorted carbon nanotube network devices. *ACS Nano* 7(1):482–490.
26. Liu H, Neal AT, Ye PD (2012) Channel length scaling of MoS₂ MOSFETs. *ACS Nano* 6(10):8563–8569.
27. Mak KF, et al. (2013) Tightly bound trions in monolayer MoS₂. *Nat Mater* 12(3):207–211.
28. Mueller T, et al. (2010) Efficient narrow-band light emission from a single carbon nanotube p-n diode. *Nat Nanotechnol* 5(1):27–31.
29. Liu C-H, Wu C-C, Zhong Z (2011) A fully tunable single-walled carbon nanotube diode. *Nano Lett* 11(4):1782–1785.
30. Chuang S, et al. (2013) Near-ideal electrical properties of InAs/WSe₂ van der Waals heterojunction diodes. *Appl Phys Lett* 102(24):242101.
31. Mak KF, Lee C, Hone J, Shan J, Heinz TF (2010) Atomically thin MoS₂: A new direct-gap semiconductor. *Phys Rev Lett* 105(13):136805.
32. O'Connell MJ, et al. (2002) Band gap fluorescence from individual single-walled carbon nanotubes. *Science* 297(5581):593–596.
33. Sczygalski E, et al. (2013) Extrinsic and intrinsic photoresponse in monodisperse carbon nanotube thin film transistors. *Appl Phys Lett* 102(8):083104.
34. Wu C-C, et al. (2013) Elucidating the photoresponse of ultrathin MoS₂ field-effect transistors by scanning photocurrent microscopy. *J. Phys. Chem. Lett.* 4(15):2508–2513.
35. Konstantatos G, et al. (2012) Hybrid graphene-quantum dot phototransistors with ultrahigh gain. *Nat Nanotechnol* 7(6):363–368.
36. Britnell L, et al. (2013) Strong light-matter interactions in heterostructures of atomically thin films. *Science* 340(6138):1311–1314.
37. Zhang W, et al. (2013) Ultrahigh-gain phototransistors based on graphene-MoS₂ heterostructures. arXiv preprint arXiv:1302.1230.
38. Rauch T, et al. (2009) Near-infrared imaging with quantum-dot-sensitized organic photodiodes. *Nat Photonics* 3(6):332–336.
39. Li Y, Xu C-Y, Zhen L (2013) Surface potential and interlayer screening effects of few-layer MoS₂ nanoflakes. *Appl Phys Lett* 102(14):143110.
40. Konstantatos G, Sargent EH (2010) Nanostructured materials for photon detection. *Nat Nanotechnol* 5(6):391–400.
41. Green AA, Hersam MC (2011) Nearly single-chirality single-walled carbon nanotubes produced via orthogonal iterative density gradient ultracentrifugation. *Adv Mater* 23(19):2185–2190.
42. Wang QH, Kalantar-Zadeh K, Kis A, Coleman JN, Strano MS (2012) Electronics and optoelectronics of two-dimensional transition metal dichalcogenides. *Nat Nanotechnol* 7(11):699–712.
43. Fang H, et al. (2013) Degenerate n-doping of few-layer transition metal dichalcogenides by potassium. *Nano Lett* 13(5):1991–1995.
44. Fang H, et al. (2012) High-performance single layered WSe₂ p-FETs with chemically doped contacts. *Nano Lett* 12(7):3788–3792.
45. Braga D, Gutiérrez Lezama I, Berger H, Morpurgo AF (2012) Quantitative determination of the band gap of WS₂ with ambipolar ionic liquid-gated transistors. *Nano Lett* 12(10):5218–5223.